Spectrum Sensing Measurements of Pilot, Energy, and Collaborative Detection

Danijela Cabric, Artem Tkachenko and Robert W. Brodersen
Berkeley Wireless Research Center, University of California, Berkeley
{danijela, artemtk, rb} @eecs.berkeley.edu

Abstract— In this paper we present an experimental study that comprehensively evaluates the performance of three different detection methods proposed for sensing of primary user signals in cognitive radios. For pilot and energy detection, our measurement results confirmed the theoretical expectations on sensing time performance. However, a physical implementation of these detectors in the presence of real noise uncertainties, analog impairments and interference allowed us to establish practical bounds on the detectable signal levels. In the case of collaborative detection, our analysis of experimental data collected in indoor environments identified the design parameters that can significantly improve the sensing gain: adaptive threshold, spatial separation and multiple antennas.

I. Introduction

The increasing demand for wireless connectivity and current crowding of unlicensed spectra has pushed the regulatory agencies to be more aggressive in providing new ways to use spectra. Cognitive Radios have been proposed as a possible solution to improve spectrum utilization via opportunistic spectrum sharing. Cognitive Radios are considered lower priority or secondary users of spectrum allocated to a primary user. Their fundamental requirement is to avoid interference to potential primary users in their vicinity.

Spectrum sensing has been identified as a key enabling functionality to ensure that cognitive radios would not interfere with primary users, by reliably detecting primary user signals. In addition, reliable sensing plays a critical role on communication links of cognitive radios since it creates spectrum opportunities for them. In order to efficiently utilize the available opportunities, cognitive radios must sense frequently all degrees of freedom (time, frequency, space) while minimizing the time spent in sensing.

There is a number of spectrum sensing techniques proposed and theoretically analyzed in the literature. Two most prominent digital signal processing techniques include coherent pilot detection that optimally detects known primary user signals and simple non-coherent energy detection applicable to any signal type [1]. In addition, a network layer technique based on collaborative detection [2], where users combine their spectrum sensing measurements, has been proposed to overcome severe fading conditions and relax signal processing requirements. However, there is a lack of experimental data that shows the feasibility and practical performance limits of these approaches under real noise and interference sources in wireless channels.

The goal of our study was to characterize and experimentally evaluate these three detection methods with respect to:

-Minimum detectable signal levels and required sensing time needed to achieve the desired probability of detection and false alarm in AWGN;

-Robustness to noise uncertainty, analog impairments, and background interference; Implementation complexity and feasibility;

-Improvements offered by number of collaborative radios, different fusion and threshold rules, spatial separation between radios, and number of antennas;

The paper is organized as follows: Section 2 reviews the pilot detection performance, addresses the limitations and provides measurement data for noise channels. In section 3, we discuss energy detection performance, implementation choices, limitation due to noise uncertainty and present the experimental data for noise channel. In section 4, we discuss the collaborative detection gains in fading channels and report the experimental data for indoor environments. Summary of the work and conclusions are presented in Section 5.

II. Pilot Detection

A. Theoretical Analysis

We consider the detection of weak deterministic signals in additive noise. The signal power is confined inside *a priori* known bandwidth B around central frequency f_c (Figure 1). We assume that activity outside of this band is unknown. In addition, we assume that primary user transmitter sends a pilot signal simultaneously with data. The sensing receiver has a perfect knowledge of the pilot signal and can perform its coherent processing. A special case of a pilot signal, frequently present in primary user systems, is a sinewave tone used for receiver synchronization. The power of the pilot tone is typically 1% to 10% of the total transmitted power.

Given the complete knowledge about the pilot at the

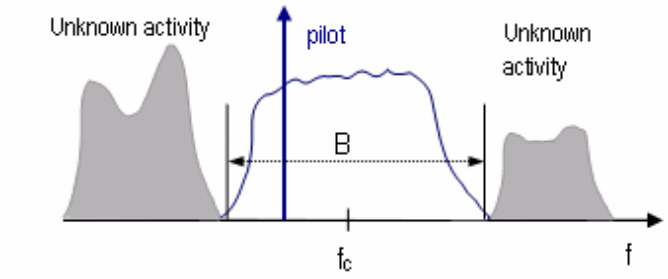

Figure 1. Spectrum Picture

sensing receiver, we consider the baseband equivalent discrete time signal model in additive white Gaussian noise (AWGN). The detection is the test of the following two hypotheses:

H_0: $Y[n] = W[n]$ signal absent
H_1: $Y[n] = X_p[n] + W[n]$ signal present
$n = 1, \ldots, N$; where N is observation interval (1)

$X_p[n]$ is the known pilot data with power θ and $W[n]$ is white Gaussian noise with variance σ_w^2. Commonly, the pilot signal is orthogonal to the data and can be considered independently.

The optimal detector is the matched filter that projects the received signal in the direction of the pilot:

$$T = \sum_N Y[n] X_p[n]^* \quad (2)$$

A matched filter is typically implemented in the digital domain, and its realization is illustrated in Figure 2.

It is well known that under the common detection performance criteria (most notably, the Neyman-Pearson criteria) likelihood ratio yields the optimal hypothesis testing solution and performance is measured by a resulting pair of detection and false alarm probabilities (P_d, P_{fa}). Each pair is associated with the particular threshold γ that tests the decision statistic:

$T > \gamma$ *decide signal present*
$T < \gamma$ *decide signal absent*

Under either hypothesis $Y[n]$ is jointly Gaussian random variable, and since T is a linear combination of jointly Gaussian random variables, it is also Gaussian. Thus,

$T \sim Normal(0, \sigma_w^2 \varepsilon)$ under H_0
$T \sim Normal(\varepsilon, \sigma_w^2 \varepsilon)$ under H_1

where $\varepsilon = \sum_N \left(X_p[n] \right)^2$.

Then P_d and P_{fa} can be evaluated as:

$$P_{fa} = Q\left(\frac{\gamma}{\sqrt{\varepsilon \sigma_w^2}}\right) \qquad P_d = Q\left(\frac{\gamma - \varepsilon}{\sqrt{\varepsilon \sigma_w^2}}\right) \quad (3)$$

If the number of samples used in sensing is not limited, this pilot detector can meet any desired P_d and P_{fa} simultaneously. The minimum number of samples is a function of the signal to noise ratio $SNR = \theta / \sigma_w^2$:

$$N = \left[Q^{-1}(P_{fa}) - Q^{-1}(P_d) \right]^2 SNR^{-1} \quad (4)$$

Since matched filter uses the optimal processing, it requires the minimum possible number of samples. Therefore, the scaling law of $N \sim 1/SNR$ gives a lower bound on the sensing time performance for any possible sensing detector type.

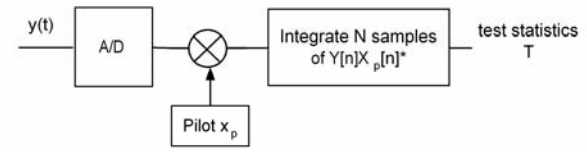

Figure 2. Pilot detection via matched filtering

B. Limitations

The theoretical analysis shows that coherent processing can turn low SNR into high SNR regime so that, given enough samples, arbitrary weak signals can be detected. However, this benefit comes at the cost of perfect synchronization required to demodulate the pilot.

Let consider the sinewave pilot: $X_p[n] = Ae^{j(w_0 n + \varphi)}$

Suppose there is a frequency offset between the primary transmitter and sensing receiver:

$$\tilde{X}_p[n] = X_p[n] e^{jwn} \quad (5)$$

Then, the decision statistic becomes:

$$\tilde{T} = \sum_N Y[n] X_p[n]^* e^{-jwn} \sim A^* e^{-j\varphi} \sum_N e^{-jwn} \quad (6)$$

If the sensing interval N becomes comparable or larger than the period of the frequency offset $(2\pi/w)$, then the decision statistic looses coherent processing gain and eventually becomes equal to zero. Therefore, in the presence of frequency offset the pilot detection has limits on sensing time and detectable signal levels.

In order to remedy the frequency offset effects, the asymptotically optimal processing involves block by block processing of coherent portions of the signal:

$$T = \sum_{n=1}^{M} \left[\sum_{k=1}^{N_c} Y[n] \tilde{X}_p[nN_c + k] \right]^2 \quad (7)$$

where $N_c << (2\pi/w)$ is the number of samples in each coherent block, and M is the number of blocks over which the sensing is performed. Now, the total number of samples is $N = M * N_c$. Note that due to non-coherent averaging of coherent blocks the scaling law would be worse than $N \sim 1/SNR$.

C. Experimental Setup

The need for experiments is stressed by the inability to realistically model all noise sources and impairments encountered in the receiver and interference environment. In addition, a comprehensive evaluation of P_d and P_{fa} requires extensive Monte Carlo simulations. Therefore, the implementation on a real-time testbed allows us to perform a large set of experiments for various signal levels and receiver settings.

The testbed used in the experiments is built around the Berkeley Emulation Engine 2 (BEE2), used for implementation of signal processing algorithms and data acquisition in real-time. The radio front-end system operates in 2.4 GHz ISM band over 85 MHz of bandwidth with programmable center frequency and several gain control stages. Reference oscillator can be generated using on board PLL or fed externally via SMA cable. The analog/baseband board contains a 14-bit 128 MHz D/A converters, 12-bit 64 MHz A/D converters, and 32 MHz wide baseband filters. For the transmitter, we used Agilent EE4438C ESG vector signal generator. For detailed testbed description and configuration setting please refer to [5].

To measure the performance under AWGN we connect signal generator to the RF board antenna input via SMA cable. The pilot signal used for testing is a sinewave carrier at 2.493GHz. The radio is put inside the RF shield, thus the only noise sources come from the radio circuitry. In order to achieve the perfect synchronization, an external RF reference from another vector signal generator was fed to the mixer of down-conversion receiver. Note that this is an idealistic situation and, in practice, the receiver would need to perform additional synchronization.

D. Measurement Results

Figure 3 shows how the sensing time required to meet fixed P_d and P_{fa} scales with the input signal level. We measured performance for three different frequency offsets: 0Hz, 10Hz, and 100Hz. In the case of perfect synchronization, measurements show complete agreement with the theoretical results and scaling law of *N~1/SNR*. As a result, extremely weak signals measured up to -136dBm can be detected. However, in the presence of frequency offsets coherent processing gains are limited by the processing time. For example, given a 10Hz frequency offset, if the receiver sense longer than 30ms, it can never meet the desired P_d and P_{fa}. Similarly, for a 100Hz offset sensing times are limited to 3ms. Due to sensing time constraints, signal levels below -132dBm and -120dBm can not be detected in the presence of 10Hz and 100Hz, respectively. We say that the receiver hits the SNR wall when the detection of weaker signals is not possible.

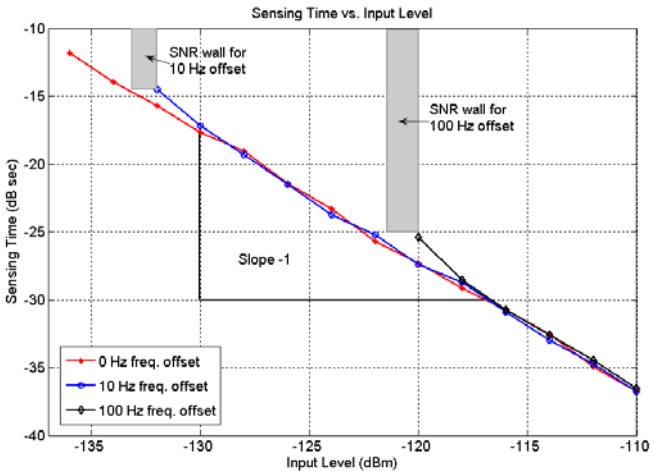

Figure 3. Required sensing time vs. input signal level for fixed Pd and Pfa for sinewave pilot in the presence of frequency offset.

III. Energy Detection

A. Theoretical Analysis

In some cases, an optimal detector based on matched filter is not an option since it would require the knowledge of the pilot data and perfect synchronization for coherent processing. Instead a suboptimal and simple energy detector is adopted, which can be applied to any signal type. Conventional energy detector consists of a low pass filter to reject out of band noise and adjacent signals, Nyquist sampling A/D converter, square-law device and integrator (Figure 4 a).

Without loss of generality, we can consider a complex baseband equivalent of the energy detector. The detection is the test of the following two hypotheses:

H_0: $Y[n] = W[n]$ signal absent

H_1: $Y[n] = X[n] + W[n]$ signal present

$n = 1, \ldots, N$; where N is observation interval (8)

The noise samples $W[n]$ are assumed to be additive, white and Gaussian (AWGN) with zero mean and variance σ_w^2. In the absence of coherent detection, the signal samples $X[n]$ can also be modeled as Gaussian random process with variance σ_x^2. Note that over-sampling would correlate noise samples and, in principle, the model could be always reduced to (8).

A decision statistic for energy detector is:

$$T = \sum_{N} (Y[n])^2 \quad (9)$$

Note that for a given signal bandwidth B, a pre-filter matched to the bandwidth of the signal needs to be applied. This implementation is quite inflexible, particularly in the case of narrowband signals and sinewaves. An alternative approach could be devised by using a periodogram to estimate the spectrum via squared magnitude of the FFT, as depicted in Figure 4 b). This architecture also provides the flexibility to process wider bandwidths and sense multiple signals simultaneously. As a consequence, an arbitrary bandwidth of the modulated signal could be processed by selecting corresponding frequency bins in the periodogram.

In this architecture, we have two degrees of freedom to improve the signal detection. The frequency resolution of the FFT increases with the number of points K (equivalent to changing the analog pre-filter), which effectively increases the sensing time. In addition, increasing the number of averages N also improves the estimate of the signal energy. In practice, it is common to choose a fixed FFT size to meet the desired resolution with a moderate complexity and low latency. Then, the number of spectral averages becomes the parameter used to meet the detector performance goal. We consider this approach in our experiments.

If the number of samples used in sensing is not limited, an energy detector can meet any desired P_d and P_{fa} simultaneously. The minimum number of samples is a function of the signal to noise ratio $SNR = \sigma_x^2 / \sigma_w^2$:

$$N = 2\left[(Q^{-1}(P_{fa}) - Q^{-1}(P_d))SNR^{-1} - Q^{-1}(P_d)\right]^2 \quad (10)$$

In the low $SNR << 1$ regime, number of samples required

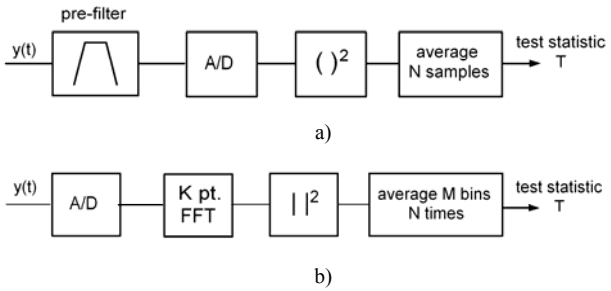

Figure 4. a) Implementation with analog pre-filter and square-law device b) implementation using periodogram: FFT magnitude squared and averaging

for the detection, that meets specified P_d and P_{fa}, scales as $O(1/SNR^2)$. This inverse quadratic scaling is significantly inferior to the optimum matched filter detector whose sensing time scales as $O(1/SNR)$.

The exception is the sinewave case where the optimum matched filter derived in section 2 can be realized using the FFT with the length equal to the multiple of a sinewave period. However, the implementation in Figure 4 b) does not implement the matched filter but rather processing derived in equation (7). Due to partially coherent processing it is expected that the sensing time scales better than $O(1/SNR^2)$ for sinewave energy detection. This detector is also robust to frequency and Doppler offsets.

B. Limitations

Unfortunately, an increased sensing time is not the only disadvantage of the energy detector. More importantly, there is a minimum SNR below which signal cannot be detected, and when the formula (10) no longer holds. This minimum SNR level is referred to SNR_{wall} [3]. In order to understand when the detection becomes impossible we need to revisit our signal model. There, we have made two very strong assumptions (that are typically made in communications system analysis). First, we assumed that noise is white, additive and Gaussian, with zero mean and known variance. However, noise is an aggregation of various sources including not only thermal noise at the receiver and underlined circuits, but also interference due to nearby unintended emissions, weak signals from transmitters very far away, etc. Second, we assumed that noise variance is precisely known to the receiver, so that the threshold can be set accordingly. However, this is practically impossible as noise could vary over time due to temperature change, ambient interference, filtering, etc. Even if the receiver estimates it, there is a resulting estimation error due to limited amount of time. Therefore, our model needs to incorporate the measure of noise variance uncertainty.

How does the noise uncertainty affect detection of signals in low SNR? Essentially, setting the threshold too high based on the wrong noise variance, would never allow the signal to be detected. If there is a x dB noise uncertainty, then the detection is impossible below $SNR_{wall}=10\log_{10}[10^{(x/10)}-1]$dB [3]. For example, if there is a 0.03 dB uncertainty in the noise variance, then the signal in -21dB SNR cannot be detected using the energy detector.

C. Experimental Setup

The goal of experimental study for energy detector was to find the scaling law of FFT based processing for different FFT sizes and signal types. The energy detector from Figure 4 b) is implemented on BEE2 using 256 and 1024 point FFT. Due to A/D sampling at 64 MHz, these two implementations have 250 kHz and 62.5 kHz FFT bin resolution, respectively. The number of spectral averages is programmable from 200 (3.2 ms) to 52,000 (0.83 s). Prior to all experiments, we calibrated the noise level of the radio receiver, and the measured level is -97 dBm in a 250 kHz and -103 dBm in a 62.5 kHz FFT bins, respectively.

We tested two types of signals: sinewave carrier at 2.493GHz, and 4 MHz wide QPSK signal centered at the same carrier. For sinewave carrier we swept signal levels from -110 dBm to -128 dBm, which is equivalent to -7 to -25 dB of the receiver *SNR* in the case of 1024 pt. FFT implementation. For 4 MHz QPSK signal, we tested levels from -98 dBm to -110 dBm, which is equivalent to -13 to -25 dB of the receiver *SNR*.

In order to accurately estimate the P_d and P_{fa} we repeated each detection measurement 1000 times. For each signal level, we collected two sets of energy detector outputs: one in the presence, and the other in the absence of the signal generator output signal. From "no input signal" data, we estimated the detection threshold to meet the specified probability of false alarm. Then, we applied the threshold to the data where signal was present and computed the probability of detection.

D. Measurement Results

Figure 5 a) shows how the sensing time scales with input signal level for QPSK signal sensing. The scaling law of

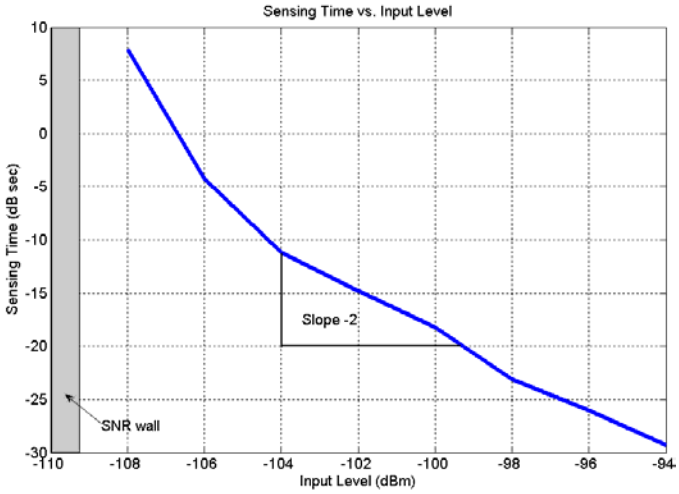

a) QPSK sensing

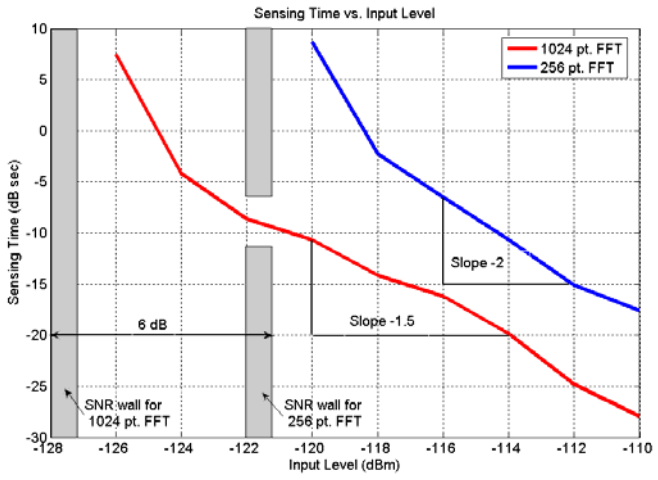

b) Sinewave sensing

Figure 5. Required sensing time vs. signal input level for fixed P_d and P_{fa}

$N \sim 1/SNR^2$ consistent with our theoretical expectation is observed for both FFT sizes. Measurements also show that when the signal becomes too weak, increasing the number of averages does not improve the detection. This result is expected and is explained by the SNR_{wall} existence. The limit happens at -110dBm (SNR_{wall}=-25dBm). From the theoretical analysis, we know that SNR_{wall}=-25dB corresponds to less than 0.03 dB of noise uncertainty. This uncertainty comes from the limited estimation time and temperature variability during the length of the experiment.

Results for sinewave energy detection show interesting behavior (Figure 5 b). First, we notice that increasing the FFT size improves the slope of the scaling law. For 1024 pt. FFT we obtained $N \sim 1/SNR^{1.5}$. This is expected since our implementation has a partial coherent processing gain for sinewave detection. Theoretically, for the FFT size of N we would get $N \sim 1/SNR$. For 256 pt. FFT coherent gain is negligible and we observe scaling law of $N \sim 1/SNR^2$.

Although there is an improved sensing time for sinewave sensing, the non-coherent processing in this implementation makes it sensitive to noise uncertainty. In the case of 1024 pt FFT, beyond -124 dBm signal level the slope becomes increasingly steep. Signals below -128 dBm cannot be detected, resulting in the SNR_{wall}=-25dB. The SNR_{wall} for 256 pt. FFT happens for signal levels lower than -122 dBm. As expected, there is a 6dB improvement in SNR_{wall} going from 256 pt. to 1024 pt. FFT as a consequence of 4 times longer coherent processing time.

IV. Collaborative Detection

A. Gains

Up to this point we have considered spectrum sensing performed by a single radio in AWGN-like channels. In fading channels, however, single radio sensing requirements are set by the worst case channel conditions introduced by multipath, shadowing and local interference. These conditions could easily result in SNR regimes below the SNR_{wall}, where the detection will not be possible. However, due to variability of signal strength at various locations, this worst case condition could be avoided if multiple radios share their individual sensing measurements [2].

Under independent fading conditions often assumed for multipath, if radios are more than λ/2 apart, cooperation can be studied as a diversity gain in multiple antenna channels. Due to a small overhead in the protocol, we consider a hard decision combining, where each radio sends its local decision to a centralized location (0 signal is absent, 1 signal is present), and the decisions is made via OR operation. It has been shown [2] that if n radios combine independent measurements, then probability of detection of the system Q_D monotonically increases as $Q_D=1-(1-P_d)^n$. In addition, the probability of false alarm for the system Q_F also monotonically increases as $Q_F=1-(1-P_{fa})^n$.

B. Limitations

Recall the single radio analysis where we identified the SNR_{wall} due to noise uncertainty and its impact on the detection threshold. Now, in the cooperation case, radios could use two different types of threshold rules in the local decision process: 1) a predetermined (fixed) threshold set by the centralized processor or 2) an independently estimated threshold based on the local noise and interference measurements. In the case of stationary environments with all radios being identical, these two rules would result in the same system performance. However, due to the presence of ambient interference caused by primary or cognitive radios in the vicinity, and local noise, temperature, and circuit variability, each radio sees different aggregate noise and interference. This observation suggests that a fixed threshold might be suboptimal, and that in practical situations the estimated threshold would provide robustness and better gains. Through experiments, we analyze benefits of noise and interference estimation, and the gap between the two threshold rules.

The collaboration gain is maximized if the radios exhibit independent fading channels. However, fading could be caused by shadowing that exhibits high correlation if two radios are blocked by the same obstacle. Commonly, a

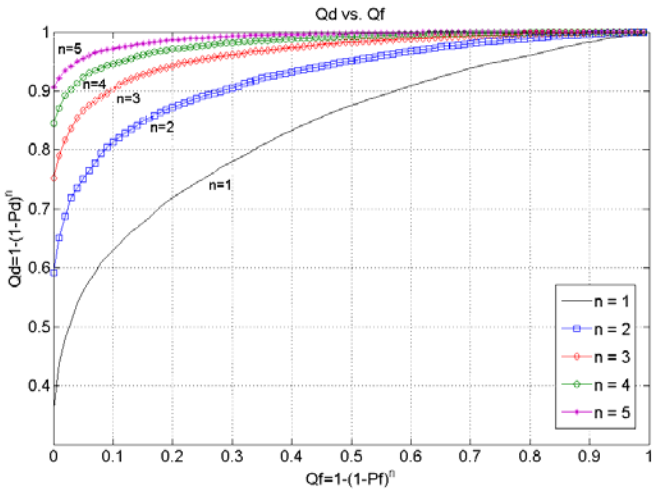

a) Sinewave sensing

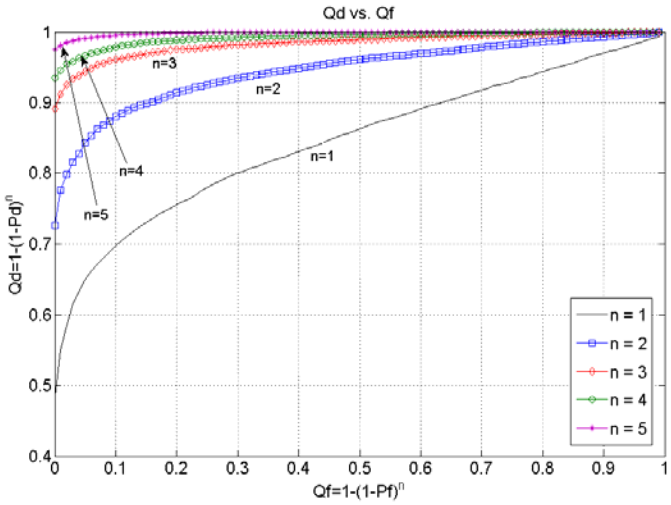

b) QPSK sensing

Figure 6. Collaborative gains vs. number of collaborative radios

shadowing correlation is described by the coefficient ρ and modeled as an exponential function of distance: $\rho=e^{-ad}$. Measurements of the shadowing in indoor environments [4] show that the correlation coefficient is independent of wavelength over a frequency octave, but it is dependent on the topography. It was estimated [4] that 90% correlation distance is typically 1m, 50 % is around 2m, and slowly decays to 30% over 8m. Therefore, in the limited area, increasing the number of radios introduces the correlation, which in effect limits the collaborative gain [2].

While large separation between radios combats shadowing, increasing the number of antennas in one radio can improve sensing via beamforming. Multiple antenna channel measurements [6] show that in most indoor environments a received signal is distributed in 1 to 3 spatial clusters. Then, the sensing receiver can exploit this channel diversity by increasing the antenna gain in the primary signal direction. Note that multiple antenna gain is easier to extract since the radios do not need ranging to identify independent collaborators. We investigate how this gain scales with number of antennas and distance between them.

C. Experimental Setup

The experiments were conducted inside the Berkeley Wireless Research Center at 54 locations on a 2m by 2m grid that covers a cubicle area, library and conference room. In all experiments, the transmitter was located inside the lab. Therefore, the signal path between the transmitter and all receiver positions included propagation through either concrete or wooden walls, supporting beams, medium and large size metal cabinets and general office furniture. The area covers a balanced variation of obstacles which are typical for indoor non-line-of-sight environments.

Due to operation in the unlicensed ISM band, outside interference had to be considered. All 802.11 b/g, Bluetooth, and ZigBee equipment was shut down during the experimentation, in order to minimize potential interference. For the sinewave, the signal generator transmitted a -40 dBm signal at 2.485GHz. For the 4 MHz wide QPSK signal, the signal generator transmitted a -30 dBm signal in 2.483GHz – 2.487GHz band, centered at 2.485GHz. The bandwidth ratio of QPSK signal to sinewave is approximately $10*1\log_{10}(4\text{ MHz}/62.5\text{kHz})=18$ dB, thus a 10 dB difference in transmit power favors the sinewave case in terms of the receiver SNR. It was expected that sinewave performance would be more affected by multipath, thus 8 dB power gain was added.

For each sensing location, data was collected for three different transmitter configurations: idle spectrum i.e. no signal, sinewave signal and QPSK signal. The idle spectrum was sensed in order to be able to compare two different threshold rules described in the previous sections. For each location and data type, spectrum was sensed 200 consecutive times using 3200 averages (51.2 ms) in the periodogram.

D. Measurement Results

First, we analyzed the collaborative gain as function of the number of collaborating radios. Figures 6 a) and b) show the system ROCs for sinewave and wideband QPSK signals, respectively. For a given probability of false alarm for the cooperating system Q_F, an estimated threshold was computed for each location based on the idle spectrum data. Then, these thresholds were used to compute the probability of detection for each location. By applying the OR function to decisions of n radios and averaging across all possible combination of n radios among 54 locations, we obtain Q_D.

For the sinewave signal, the single radio sensing is limited by multipath fading, thus significant improvement is achieved even with 2 cooperative radios. Given 10% probability of false alarm, an 18% improvement is observed through cooperation of two radios, then 9% for 3, and it saturates to 4% and 3% for 4 and 5 cooperating radios, respectively. Overall, going from 1 to 5 collaborative radios detection improves from 63% to 97%. Note that if radios would experience the independent multipaths then the cooperation would result in $Q_D=1-(1-0.63)^5=99\%$. In the case of wideband QPSK signal, the probability of detection is even better, though the average SNR is 8dB lower. With 5 collaborative radios, Q_D for QPSK reaches 99%. This improvement in the QPSK sensing is due to frequency diversity gain, which makes the wideband signal less sensitive to deep fades.

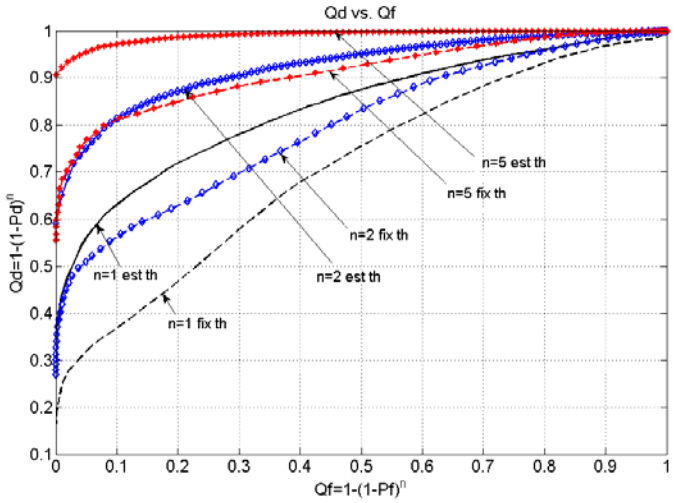

Figure 7. Collaborative gains vs. threshold rule

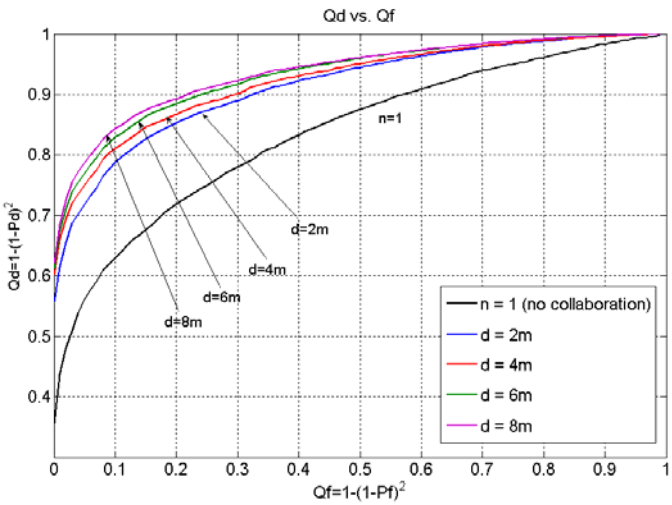

Figure 8. Large scale collaborative gain

Then, we compared experimental results for two different threshold rules applied to the same set of measurement data. For the fixed threshold rule, the same threshold is applied for all possible combinations of cooperating radios. As expected, Figure 7 shows that the performance of the fixed threshold rule is significantly lower than that of the estimated threshold rule. Even for the single radio sensing under variable noise and interference, it is essential to apply the location and time relevant threshold obtained via estimation. The cooperation gains are still present, but are significantly reduced by suboptimal threshold rule. The gap between the two rules varies form 15% to 25%. Thus, even a moderate Q_D=90 % and Q_F=10% can never be met using the fixed threshold. The implications of this result imply that robust sensing must involve frequent receiver noise calibration and accurate interference estimation. In turn, this might require additional sensing time and more complex sensing receiver.

Next, we analyzed the effect of spatial correlation on the Q_D and Q_F for two cooperating radios. Measurements in Figure 8 show that the Q_D monotonically increases as the separation between two cooperating radios increases. The improvement of up to 7% in Q_D is obtained once the cooperation distances extend to 8 m. Therefore, it is beneficial to increase the radio separation so that correlation coefficient is less than 10%, which for this particular environment happens at 8 m distances.

Lastly, we picked one location with poor Q_D and Q_F and measured how much they can be improved by multiple antennas. Figure 9 a) shows that it is beneficial to space the antennas at distances larger than λ/2 (12cm) to maximize the gain. Then, we measured how the performance scales with the number of antennas. Results in Figure 9 b) show that 2 antennas improve Q_D by 10% and 4 antennas maximize it by 25% gain. However, the gain is also saturated with 4 antennas, and there is no benefit in adding more. This is explained by limited number of degrees of freedom, i.e. spatial clusters in indoor channels.

V. Conclusions

In this paper we presented an experimental study that comprehensively evaluates the performance and limitations of three different detection methods proposed for sensing of primary user signals in cognitive radios. The pilot detection requires minimum amount of time for sensing but requires perfect synchronization, thus it is highly susceptible to frequency offsets. The energy detection requires the longest processing time and suffers from noise uncertainties that put limits on minimum detectable signal levels. We proposed the efficient implementation using FFT that offers signal processing gains for energy detection of sinewave pilot signals. Our study of collaborative detection quantified performance gains with respect to number of radios and their spatial separation in indoor environments. We also identified the robust threshold rule for hard decision combining. Lastly, we showed the sensing gains offered by multiple antennas.

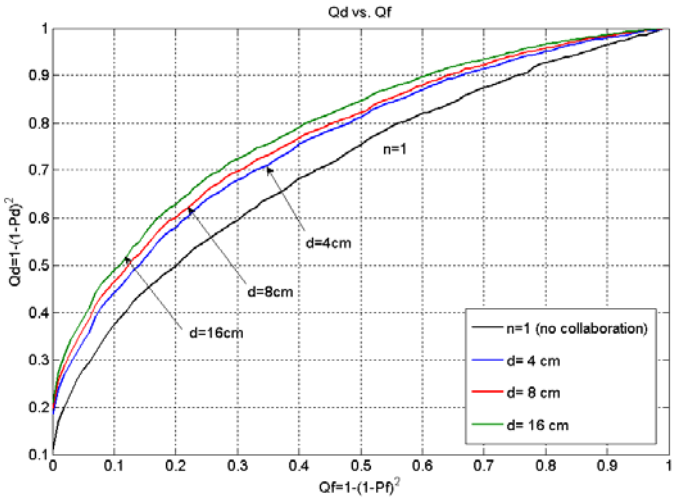

a) Impact of spatial separation

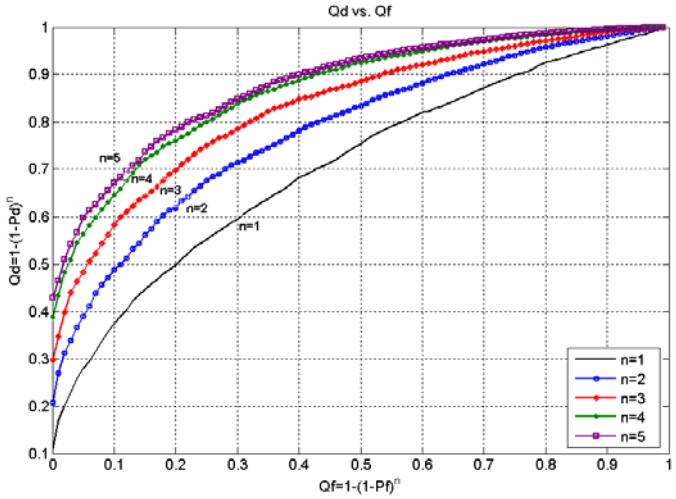

b) Impact of number of antennas

Figure 9. Small scale collaborative gain and benefit of multiple antennas

Acknowledgement

This work has been supported by MARCO fund (C2S2) under contract 2003-CT-888 and BWRC industry members.

References

[1] D. Cabric. S.M. Mishra. R.W. Brodersen, "Implementation Issues in Spectrum Sensing", In Asilomar Conference on Signal, Systems and Computers, November 2004.

[2] A. Ghasemi, E.S. Sousa, "Collaborative Spectrum Sensing for Opportunistic Access in Fading Environments", In proc. of DySPAN'05, November 2005.

[3] R. Tandra, A. Sahai. "Fundamental Limits on Detection in Low SNR", In proc. of the WirelessComm05 Symposium on Signal Processing, June 2005.

[4] J.C. Liberti, T.S. Rappaport, "Statistics of shadowing in indoor radio channels at 900 and 1900 MHz", In proc. of Military Communications Conference, MILCOM'92, October 1992.

[5] D. Cabric, A. Tkachenko, R.W. Brodersen, "Experimental Study of Spectrum Sensing based on Energy Detection and Network Cooperation", in Proc. of 1st Intl. Workshop on Technology and Policy for Accessing Spectrum (TAPAS 2006), Boston, August 2006.

[6] A. Poon, M. Ho, "Indoor Multiple Antenna Characterization from 2 to 8 GHz", In proc. of International Conference on Communications, ICC'04, June 2004.